NINTH EUROPEAN ROTORCRAFT FORUM

Paper No. 55

ROTOR DYNAMIC INFLOW DERIVATIVES AND TIME CONSTANTS FROM VARIOUS INFLOW MODELS

Dale M. Pitt

McDonnell Aircraft Company
St. Louis, Missouri 63166 USA

and

David A. Peters

Washington University
St. Louis, Missouri 63130 USA

September 13-15, 1983

STRESA, ITALY

Associazione Industrie Aerospaziali

Associazione Italiana di Aeronautica ed Astronautica

ROTOR DYNAMIC INFLOW DERIVATIVES AND

TIME CONSTANTS FROM VARIOUS INFLOW MODELS

Dale M. Pitt
McDonnell Aircraft Company
St. Louis, Missouri 63166 USA

David A. Peters
Washington University
St. Louis, Missouri 63130 USA

ABSTRACT

In recent work, an actuator-disc theory was used to obtain the dynamic inflow derivatives for rotors. The fundamental assumptions of that work are examined in the present research through comparisons with more sophisticated induced-flow descriptions. One description involves a general, unsteady actuator-disc; and the other involves a prescribed-wake, discrete-vortex analysis of a four-bladed rotor. The results reveal the strengths and weakness of previous formulations.

1. Introduction

It has been known since the early days of the helicopter that the induced flow field of a rotor responds in a dynamic fashion to changes in control settings, blade motions, or hub motions. The dynamic character of the rotor wake implies that the expected rotor dynamics can be significantly altered due to angle-of-attack changes created by the transients in induced flow. The mathematical modeling of induced-flow response has been called *the theory of dynamic inflow*.

The early work in dynamic inflow, References 1-5, starts with Amer noting that the pitch and roll damping of a rotor depend on the blade pitch setting.[1] Subsequently, Sissingh[2] used a quasi-steady momentum theory, where he assumed the induced flow transients instantaneously follow the lift transients, to describe the dynamic inflow experiences of Amer. In particular, the change in pitching moment due to pitch rate (the pitch damping) creates a corresponding change in the induced flow field which, in turn, alters the development of that pitch moment. In Reference 3, however, Carpenter and Fridovitch show that there is a measurable time lag between the inception of blade life and the subsequent development of induced flow. They quantitatively explained the time lag in terms of the apparent mass of the induced flow (as approximated by the apparent mass of an impermeable disk in still air). Similar work by Rebont corroborates the results in Reference 3, but he must double the apparent mass used in Reference 3 in order to correlate his own experimental data with analysis.[4] In the unsteady aerodynamic theory of Loewy,[5] the vortex system of the rotor is treated by layers of vorticity; and a Theodorsen-type Lift-Deficiency Function is obtained. In the limit of zero reduced frequency, such a theory produces a quasi-steady inflow theory for climb; and, if exercised at moderate reduced frequencies, it could conceivably provide apparent mass terms.

More recently Shupe[6] shows that the Sissingh model is equivalent to the use of a reduced Lock number (i.e. a lift-deficiency function) for cyclic modes. In addition, the reference attempts to extend the dynamic-inflow model into the forward-flight regime. Lastly, he introduces the inflow dynamics as an integral component of rotor aeroelasticity and rotor-body stability modeling.

Ormiston and Peters compare theoretical and experimental values of steady control derivatives under various quasi-steady inflow assumptions.[7] The results for hover corroborate earlier findings that quasi-steady momentum theory is adequate. The results for forward flight, however, show large discrepancies between theory and experiment. In response to this discrepancy, Ormiston and Peters postulate a more general formulation of the inflow law; it assumes that three induced-flow distributions (uniform, fore-to-aft, and side-to-side) are linear functions of three aerodynamic loading conditions (thrust, pitch moment, and roll moment). Unlike the previous theory, however, the new one allows for all possible linear couplings between loads and inflow (9 derivatives), whereas the old theory allows no couplings (3 derivatives). An empirical flow model is used to successfully correlate hover and forward flight data.

In References 8-10, the theory of dynamic inflow progresses from a quasi-steady theory into a truly unsteady formulation. Crews, Hohenemser, and Ormiston introduce a dynamic-inflow model for hover that includes three uncoupled, first-order equations that describe the magnitude of the induced flow distributions (uniform, fore-to-aft, and side-to-side).[8] The gains and time constants in these three equations are chosen on the basis of correlation with experimental frequency-response data (as in Reference 7). It is interesting that even though Reference 8 does not consider the work of Reference 3, the identified time constant for cyclic modes in Reference 8 is within 1% of the value that would result from the apparent inertia of an impermeable disc, as outlined in Reference 3. Peters[9] introduces the apparent mass terms of Reference 3 into both the momentum-theory formulation of Reference 2 and the empirical formulation of Reference 7. The results are used to correlate rotor frequency response (to both hub and swashplate inputs) in hover and forward flight. In hover, the apparent-mass terms with momentum theory provide excellent correlations. Furthermore, the same apparent mass terms, when combined with the empirical model, give equally good correlation in forward flight, despite the fact that the empirical model is identified only on the basis of hover data. In addition, Reference 9 formulates the momentum theory in a unified way that allows smooth transitions between hover, climb, and forward flight. Finally, Banerjee, Crews, and Hohenemser[10] attempt parameter identification of the entire 3X3 inflow matrix from transient rotor data, but no clear conclusions are reached.

The effect of dynamic inflow on rotor stability and transient response are investigated in Reference 11-14. Ormiston studies the hover dynamics of a three-bladed rotor with dynamic-inflow degrees of freedom (three second-order rotor equations plus three first-order inflow equations).[11] He finds that the reduced Lock number approximation is adequate for the regressing mode but not for the collective and progressing modes. Peters and Gaonkar include dynamic inflow for rotor flap-lag dynamics in hover and forward flight.[12] They find that, with an inplane degree of freedom, one must define an equivalent Lock number <u>and</u> an equivalent profile drag coefficient in order to approximate the damping of regressing modes. Finally, Peters and Gaonkar[13] and Johnson[14] show that dynamic inflow accounts for most of the observed discrepancies between theory and experiment for air and ground-resonance dynamics of helicopters in hover.

It is obvious from the previous work that dynamic inflow is important in rotor dynamic and stability analysis. A requirement still exists for a unified dynamic inflow theory that would adequately model both hover and forward flight. There are several recent investigations of rotor inflow that contain the ingredients necessary for an adequate quasi-steady model. In each case, however, the investigations concentrate on the steady rotor loads and inflow; but they do not investigate the consequences on the induced flow of systematic load perturbations. Joglekar and Loewy find relationships between rotor loads and induced flow from a potential-flow model of a pressure discontinuity across an actuator disc.[15] Landgrebe models the induced flow by a discrete representation of rotor shed vorticity, and he allows for either a prescribed wake or a free wake.[16] Ormiston uses a simple actuator-disc theory coupled with rigid blade dynamics to estimate rotor induced flow.[17]

Pitt and Peters take the actuator-disc model in Reference 15 and extend it, as necessary, in order to formulate a general, quasi-steady inflow theory. In particular, the authors perform the necessary integrations of the loads and induced flow and develop closed-form expressions for the 9 elements of the inflow-derivative matrix, [L]. The elements of [L] are found as functions of the free-stream velocity (air speed plus average, steady induced flow) and the disc angle-of-attack (90^o for hover, 0^o for edgewise flight).

Before making a final conclusion on the universality of the Pitt/Peters model, there are two major assumptions in Reference 18 that must be critically examined. First, there is the assumption that a rotor can be modeled as an actuator disc. To test this assumption, the quasi-steady inflow model needs to be compared with an analysis that includes the vortices shed by each individual blade. Second, there is the superposition assumption which (as shown in Reference 18) is equivalent to the assumption that all velocities are in-phase. To test this assumption, we must compare results with a more sophisticated analysis that does not assume in-phase velocities. It is the purpose of this paper to test these assumptions in the manner indicated above. Finally, to complete the development of this dynamic inflow model, the results in Reference 18 will be generalized so as to be applicable to nonlinear analyses. It should be noted that the results presented here are based on a Doctor of Science Thesis by the first author under the direction of the second.[19]

2. Mathematical Formulation of Inflow Models

The details of the actuator-disc models are given in References 18 and 19, but the basic equations will be repeated for clarity. First, the nondimensional induced flow is represented by five assumed inflow distributions with undetermined magnitudes.

$$\nu = \nu_o + \nu_s \bar{r}\sin\psi + \nu_c \bar{r}\cos\psi + \nu_{2s}\bar{r}^2\sin 2\psi + \nu_{2c}\bar{r}^2\cos 2\psi \qquad (1)$$

The first term, ν_o, represents a uniform distribution; the second term, ν_s, represents a side-to-side distribution; the third term, ν_c, represents a fore-to-aft distribution; and the last two terms represent second-harmonic inflow variations. The induced-flow distributions in equation (1) are assumed to be linear functions of five generalized loadings on the rotor. These loading factors are defined in terms of nondimensional coefficients expressed as integrals of the disc loading per unit area, $F(r,\psi)$.

$$C_T = \frac{1}{\rho\pi\Omega^2R^4}\int_o^{2\pi}\int_o^R Frdrd\psi$$

$$C_L = -\frac{1}{\rho\pi\Omega^2R^5}\int_o^{2\pi}\int_o^R Fr^2\sin\psi drd\psi$$

$$C_M = -\frac{1}{\rho\pi\Omega^2R^5}\int_o^{2\pi}\int_o^R Fr^2\cos\psi drd\psi$$

$$C_{2L} = -\frac{1}{\rho\pi\Omega^2R^6}\int_o^{2\pi}\int_o^R Fr^3\sin 2\psi drd\psi \qquad (2)$$

$$C_{2M} = -\frac{1}{\rho\pi\Omega^2R^4}\int_o^{2\pi}\int_o^R Fr^3\cos 2\psi drd\psi$$

Other radial weightings and higher harmonics are possible; but these have physical significance as well as mathematical simplicity.

If we now define a vector of induced-flow coefficients $\{\nu\}$ and a vector of loading conditions $\{F\}$

$$\nu \equiv \begin{Bmatrix} \nu_o \\ \nu_s \\ \nu_c \\ \nu_{2s} \\ \nu_{2c} \end{Bmatrix}, \qquad F \equiv \begin{Bmatrix} C_T \\ C_L \\ C_M \\ C_{2L} \\ C_{2M} \end{Bmatrix} \tag{3a,b}$$

then a general formulation of dynamic inflow can be written (for a given reduced frequency) as follows,

$$\{\nu\} = [L(K)]\{F\} \qquad \{F\} = [L(K)]^{-1}\{\nu\} \tag{4a,b}$$

where L(K) is a matrix (dependent on reduced frequency, K) that relates induced flow to loads. In general, L(K) is complex and gives both magnitude and phase. In previous work, it has been assumed that $[L(K)]^{-1}$ can be represented by a quasi-steady matrix, $[L(0)]^{-1} \equiv [L]^{-1}$, plus an apparent mass term.

$$[L(K)]^{-1} = iKv[m] + [L]^{-1} \tag{5}$$

Since $K \equiv \omega/v$, where ω is the frequency of response, equation 5 implies an induced-flow law in either of the following forms.

$$[M]\{\nu\} + [L]^{-1}\{\nu\} = \{F\} \tag{6a}$$

$$\{\nu\} + [LM]^{-1}\{\nu\} = [M]^{-1}\{F\} \tag{6b}$$

$$[LM]\{\nu\} + \{\nu\} = [L]\{F\} \tag{6c}$$

The L,M, and L(K) matrices can be found from either an analytic or an experimental representation of the rotor wake. Apply any one of the loadings in equations (2) for a given K and measure the normalized induced flow field, $\bar{q}(r,\psi)$, due to that loading. If one then extracted $\{\nu\}$ from that flow field, he would have a column of L(K). In this present paper, the extraction of the $\{\nu\}$ is accomplished by the following integrals

$$\nu_o = \frac{1}{\pi}\int_0^{2\pi}\int_0^1 \bar{q}\,\bar{r}d\bar{r}d\psi \qquad \nu_{2s} = \frac{6}{\pi}\int_0^{2\pi}\int_0^1 \bar{q}\,\bar{r}^3 \sin 2\psi d\bar{r}d\psi$$

$$\nu_s = \frac{4}{\pi}\int_0^{2\pi}\int_0^1 \bar{q}\,\bar{r}^2 \sin\psi d\bar{r}d\psi \tag{7}$$

$$\nu_{2c} = \frac{6}{\pi}\int_0^{2\pi}\int_0^1 \bar{q}\,\bar{r}^3 \cos 2\psi d\bar{r}d\psi$$

$$\nu_c = \frac{4}{\pi}\int_0^{2\pi}\int_0^1 \bar{q}\,\bar{r}^2 \cos\psi d\bar{r}d\psi$$

where $\overline{q}$ could have real and imaginary (in-phase and out-of-phase components). The computation of ν_o is clearly the average of $\overline{q}$. The other ν's are Fourier harmonics. The $\overline{r}$ weightings in equation 7 are not unique, but are consistent with the other definitions used in this work. In this present paper two versions of an actuator disc theory are used to find $\overline{q}$ for the various loading conditions, thus giving L(K). In addition, a prescribed-wake, discrete-vortex theory is used to find the quasi-steady L for comparison. The actuator-disc theory is based on pressure distributions developed by Kinner[15] that solve Laplace's equation, $\phi,_{ii} = 0$, in an ellipsoidal coordinate system and that also gives a pressure discontinuity (i.e. lift) across a circular disc. Over the area of the rotor disc, the lift density will correspond to the difference in the pressure P below and above the actuator-disc. Thus, the thrust of the rotor disc is an area integration of the lower pressure minus the upper. The thrust in the ellipsoidal coordinate system is

$$T = \sum_{\substack{m,n \\ m<n}} \rho V^2 \left[\int_0^{2\pi} (C_n^m \cos m\psi + D_n^m \sin nm\psi) d\psi \right] \int_0^R P_n^m(\nu) Q_n^m(i0) r dr \quad \text{(lower - upper)} \tag{8}$$

where P_n^m and Q_n^m are, respectively, associated Legendre functions of the first and second kinds; C_n^m and D_n^m are arbitrary constants; and ν, η, and ψ are ellipsoidal coordinates defined in reference 15 and 19. When the integration and summation of equation 8 are performed, the find value of the rotor loading (i.e., C_L, C_M, etc.), is used to evaluate the constants C_n^m and D_n^m. This process and the value of the constants are given in reference 19.

Each loading integral, equations 2 and 8, is uniquely determined by a single coefficient of the Kinner distribution and is independent of all others. Differing pressure distributions can result in identical average loadings. One of the purposes of this research is to determine if such pressure distributions will also result in identical averaged values of the induced flow. To do this, we consider two types of pressure distribution. The first, called "uncorrected", contains only the single coefficient of ϕ necessary to create the appropriate loading. The second distribution, called "corrected", includes just enough of the next-higher pressure term to enforce the conditions $\phi = 0$, $d\phi/dr = 0$, at $r = 0$, which is a reasonable distribution for a rotor. Figure 1 shows the corrected and uncorrected thrust distributions. The roll/pitching moment and higher harmonic loadings are not shown due to the brevity of this paper, but can be found in reference 18 and 19.

Using potential theory the steady velocity distribution, $\overline{W}$, due to a given pressure distribution can be determined using the Kinner pressure distribution, ϕ, as follows,

$$\overline{W}(X',Y',Z') = -v \int_0^\infty \left[\frac{-\eta(1-\nu^2)}{\nu^2+\eta^2} \cdot \frac{\partial\phi}{\partial\nu} + \frac{-\nu(1+\eta^2)}{\nu^2+\eta^2} \cdot \frac{\partial\phi}{\partial\eta} \right] d\xi \tag{9}$$

The variable ξ is a dummy variable of integration. Thus, the integration is performed from the disc to the infinite field along the streamline parallel to the X axis in the wind system where ν and η are functions of ξ. The above expression is algebraically complex and is evaluated numerically. The resulting steady induced velocities from equation 9 are integrated as in equation 7 to yield the quasi-steady L matrix.

One of the accomplishments of this present work is the extension of the above actuator-disc theory to the unsteady case. The unsteady theory is developed from the nondimensional, linearized, unsteady momentum equation as follows

$$\overset{*}{\bar{q}}_{,i} - vq_{i,x} = -\hat{\phi}_{,i}$$

where

$$\psi = \Omega t \qquad \hat{\phi} = \frac{P}{\rho\Omega^2R^2} \tag{10}$$

$$(*) = \frac{d}{d\psi} \qquad \bar{q} = \frac{q}{\Omega R}$$

$$v = \frac{V_{FS}}{\Omega R} \qquad x = X/R$$

The above equation can be solved by either of two different methods. In the first method, we assume that the pressure field can be expressed as a "mutually in-phase" simple-harmonic function. This will be referred to as "superposition of velocities". In the second method, we assume that the inflow velocities can be represented as in-phase simple harmonic motion. This will be referred to as "superposition of pressures".

In the superposition of velocities method, all the components of pressure are assumed to be in-phase. Thus, we use the complex-number notation:

$$\hat{\phi} = \bar{\phi}e^{j\omega\psi} \qquad q = \bar{q}\ e^{j\omega\psi}$$

where the pressure term $\bar{\phi}$ is assumed to be a real function. The velocity field is represented by a complex expression, $\bar{q} = w + ju$ and represents a superposit of the complex velocity field. Substitution of equations 11 and 12 into equation 10 results in the following two equations for the real and imaginary portions.

$$\omega^2u_i + v^2u_1'' = \omega\bar{\phi}_{,i}$$

(13 a & b)

$$\omega^2w_i + v^2w_1'' = v\bar{\phi}'_{,i}$$

If one takes the derivative of equations 13 a & b with respect to i and employs the continuity equation one obtains

$$\bar{\phi}_{,ii} = 0$$

i.e.

$$\nabla^2\ \bar{\phi} = 0 \tag{14}$$

Thus, we note that, for the complex frequency response problem, the pressure distribution in equation 10 must satisfy the Laplace equation, i.e. 14. This is very significant in that it allows the use of the Kinner static pressure distirbution for the unsteady theory. Equations 13 a & b can be treated by a Laplace transform in ξ followed by application of the convolution theorem. The final solution for unsteady induced flow at the rotor disc is, therefore,

$$w_{z'} = \frac{1}{v}\int_\infty^0 \bar{\phi}_{,z'}\ \cos(K\xi)d\xi \qquad \text{(in-phase)} \qquad (15\ a\ \&\ b)$$

$$u_{z'} = -\frac{1}{v}\int_\infty^0 \bar{\phi}_{,z'}\ \sin(K\xi)d\xi \qquad \text{(out-of-phase)}$$

where K is a reduced frequency based on air speed, not tip speed, $K = \omega/v$.

Several interesting aspects of these equations should be pointed out. First, these are identical to the integrals in the steady aerodynamic theory, equation 9, except for the weighting functions that have been added. (Note: $\bar{\phi}_{,z'}$ in equation 15 is equal to the bracketed term in equation 9). Second, these weighting functions, $\cos(K\xi)$ and $\sin(K\xi)$, have direct physical interpretation. They can be associated with an oscillatory pressure field that varies as a wave traveling at velocity v and frequency ω. Third, the effect of unsteadiness is only a function of K. Thus, for a given rotor angle-of-attack, a single sweep of K will suffice to give the behavior for all ω,v combinations. Lastly, the similarity of equations for the steady and unsteady induced velocities allows the utilization of the same numerical quadrature technique for either case.

The second assumption used with the solution of equation 10 is called the superposition of pressures. In this method it is assumed that the inflow distribution varies harmonically but is in-phase. Thus, the induced velocities and pressures are expressed as

$$q_i = \bar{q}_i \, e^{j\omega\psi} \qquad (16) \qquad\qquad \hat{\phi} = \bar{A} \, e^{j\omega\psi} \qquad (17)$$

where $\bar{q}$ is assumed to be a real number and the pressure distribution is represented by the complex expression, $\bar{A} = A_o + B_o j$, hence the name superposition of pressures. Substitution of equations 16 and 17 into the momentum equation 10 yields the following two equations.

$$\text{REAL COMPONENTS} \quad v\bar{q}_{i,x} = A_{o,i}$$

$$\text{IMAGINARY COMPONENTS} \quad \omega\bar{q}_i = -B_{o,i} \qquad (18\text{ a \& b})$$

when one takes the derivative of equations 18 a & b with respect to i and employs the continuity equation, one has

$$\nabla^2 B_o = 0 \qquad\qquad \nabla^2 A_o = 0 \qquad (19)$$

Thus, each pressure function (A_o or B_o) can be represented by the steady pressure series seen earlier. (They each solve the same equations and boundary conditions.) It follows directly, under the assumption of in-phase velocities, that the relationship between the induced velocities and the in-phase pressure (A_o) is identical to that of the steady theory, equation 18a. The out-of-phase pressure distribution (B_o) on the other hand, is given by equation 18b which states that the velocity equals $-1/\omega$ times the derivative of pressure (with no integration from $0 \to \infty$ as previously required). Equation 17 implies that the pressure from q and $\dot{q}$ (i.e., A_o and B_o) can be superimposed!! This has been an underlying assumption in all dynamic inflow work to date. Furthermore, since $\bar{q}_i = -1/\omega \, B_{o,i}$, the out-of-phase (apparent mass) is independent of either the magnitude or direction of the free-stream velocity (another assumption of previous work in dynamic inflow).

It is reasonable to consider the correlation between the two above theories (pressure in-phase, velocity in-phase) and the true solution. One would expect the actual case to have neither in-phase pressure nor velocity. Thus, a comparison of results under the two assumptions can be used to obtain reasonable bounds on the variability of unsteady effects.

In the superposition of velocities method, in-phase pressure field, the general form of the velocity can be written as

$$\{F\} = [L(K)]^{-1}\{\nu\} \tag{20}$$

In the superposition of pressures method, in-phase induced velocities, the general form of the equation after substituting the assumed induced velocity $\{\nu\} = \{\nu\}\bar{e}^{i\omega\psi}$ is

$$[[L]^{-1} + [M]j\omega]\ \{\nu\} = \{F\} \tag{21}$$

Thus, the unsteady aerodynamic research is concerned with the equivalence of equations 20 and 21 i.e.

$$L(K)^{-1} \overset{?}{=} [L^{-1} + Mj\omega] \tag{22}$$

A second aspect of this research is a study of the applicability of an actuator-disc analysis to a physical rotor system with a finite number of blades. To this end, we will compute the L matrix (steady case) by use of a rotor model that inlcudes blade dynamics and the finite number of blades. In particular, we use the Prescribed-Wake Program of the United Technologies Research Center, Ref. 16. This program was modified to obtain the upper 3X3 matrix (9 elements) of the L-matrix. The precedure required the independent perturbation of the collective, pitch, and roll control about a trim condition. The pertrubed induced velocity and rotor lift are integrated both radially and azimuthally to yield the perturbed vectors $\{\bar{\nu}\}$ and $\{\bar{F}\}$ with the resulting static [L] matrix

3. Results

A Fortran computer has been written to calculate both the steady and unsteady induced velocities for the actuator-disc theory. The induced velocities are integrated on the rotor disc to obtain the induced flow perturbations according to equation 7 and the L(K) matrix results from equation 4.

3.1 Steady Actuator

The first step in the numerical integration of the induced velocity equation 9 is the transformation of the disc coordinates into ellipsoidal coordinates. The integration is performed along a streamline where the polynomials $P_n^m(\nu)$ and $Q_n^m(i\eta)$ and their derivatives are evaluated at each integration point. Generally, the program integrates to a final η of 15 to 20 before the integral converges. The induced velocities are then integrated in the radial and azimuthal direction for each separate loading condition to obtain the 5X5 and 3X3 [L] matrix. See reference 19 for a more detailed account of this procedure.

As noted in reference 18, there exists two special cases for the calculation of the steady induced velocities. For these cases, $\alpha = 90^o$ and 0^o, the induced velocities are calculated by hand (in a closed-form solution) and serve as a check on the numerical accuracy of the computer program. This is an important verification since almost the identical program is used for the unsteady results.

In general, the 5X5 [L] matrix is dependent on angle-of-attack and the corrected/uncorrected pressure loadings. The 5X5 matrix can be partioned into the standard 3X3 by negating the higher harmonic loadings. The 5X5 [L] matrix and its variations with α and loading distribution are given in detail in references 18 and 19 where the first column was obtained in closed-form. Subsequently, Gaonkar et al verified the results and obtained closed-form expressions for columns 2 through 5, reference 20. These values agree with the numerical data of references 18 and 19 and are presented in table 1.

The first column of the L matrix is the induced velocity perturbations for the corrected or uncorrected thrust loading. The L(1,1) term (ν_o due to C_T) is 0.5 for the complete range of alpha and is also independent of lift distribution. This is the same value predicted by the momentum theory of reference 7. The L(3,1) term (ν_c due to C_T) is zero for the case of axial flow and as α approaches zero, the edgewise flight condition, the term exhibits a nearly linear variation. The uncorrected value of L(3,1) is approximately 60% larger than the corrected value. Interestingly, this term is zero for momentum theory, but is present in the vortex theories. Because the L(3,1) term is positive and greater than L(1,1), it implies that there is an upwash at the front of the rotor.

The L(5,1) term is the second cosine harmonic of induced flow due to thrust (ν_{2c} due to C_T). This term is zero at $\alpha = 90^o$ and displays a smooth transition to $\alpha = 0^o$. The L(5,1) changes sign as the thrust loading is varied from the corrected thrust to the uncorrected thrust distribution, consequently, the L(5,1) term is heavily dependent on the lift distribution. The uncorrected L(5,1) is always positive and is relatively large; and, for $\alpha < 10^o$, it is larger than the average value of the induced velocity, ν_o. The corrected L(5,1) is negative for all values of α up to $\alpha = 90^o$ where it is zero. A negative L(5,1) yields an upwash at the front of the rotor disc.

Due to space limitations, the results for only the first column of the [L] matrix are presented. However, the physical significance and results for each column of the matrix is discussed in detail in reference 19. The inverse of the steady L matrix is required when writing the induced flow model as shown in equation 6. The inverse matrix is also required for the unsteady induced velocity by the method of superposition of pressure. Both the 5X5 and 3X3 L matrices developed here are well-behaved and always invertiable.

3.2 Unsteady Actuator

The computer code for the steady condition is extended to perform the unsteady superposition of velocities caluclations of equation 15. The in-phase induced velocities, w, and the out-of-phase induced velocities, u, are integrated in the same manner as the steady calculations except that the weighting functions, $\cos(K\xi)$ and $\sin(K\xi)$ are included. The weighting functions cause the function $\Phi_{,z}$, to oscillate as the sine or cosine function. As the reduced frequency K is increased, the frequency of oscillation correspondingly increases. This means that the streamwise integration increment must decrease as K increases. Consequently, computer time increases with increasing K. The complex induced velocity is integrated over the rotor disc to obtain the complex [L(K)] matrix.

As in the steady case, a special case is used to verify the complex induced velocity calculations of the computer program. For axial flight, $\alpha = 90^o$, equation 15 is integrated on the disc in closed-form to yield the exact value of the apparent mass matrix [M] which are given in table 2. The computer time required for the calculation of the (S.V.) unsteady induced velocities and L(K) matrix increase drastically as α approaches 0 and K increases. These large computing times reveal the tremendous advantage that is obtained if the [L] and [M] matrices can be used rather than the complex L(K).

The first case to be presented is the case of axial or hovering flight. The complex [L(K)] matrix is a diagonal matrix for $\alpha = 90^o$, meaning that none of the elements are coupled. The $[L(K)]^{-1}$ from superposition of pressure (S.P.) is just ik $[M] + [L]^{-1}$. (Results are normalized to v = 1). This leads to a definition of apparent mass defined as 1/k Im L(K) for the superposition of velocities (S.V.) method.

Due to the limited scope of this paper, only the first column of the L(K) matrix and the apparent mass matrix will be discussed. A more detailed discussion and classification of the results is presented in reference 19. Figure 2 is a comparison of the apparent mass M(1,1) terms as calculated by the S.V. and S.P. method. The apparent mass elements calculated by the S.V. method asymptotically approach infinity as K approaches zero. This is exactly analogous to the case for an unsteady wing in which the log (K) term in the Theodorsen function gives an infinite slope at K = 0, Ref. 18. As K is increased, the apparent mass calculated by the method of S.V. exponentially approaches the apparent mass calculated by the S.P. method. At a very high frequency, figure 2 shows that the apparent mass of both methods agree. Even though there is a large difference in the apparent mass terms calculated by the superposition of pressures and velocities in the $K < 50$ range, the reduced frequency is small and consequently the imaginary terms are relatively small, and the effects of the different apparent masses are not great.

The other nonzero elements of the apparent mass matrix show similar trends as figure 2. For large values of K, i.e., $K > 250$, all the apparent mass terms predicted by the S.P. and S.V. methods agree. The values are presented in table 2. Due to the symmetry of the airflow through the rotor for axial flow, $\alpha = 90^{\circ}$, the M(2,2) and M(3,3) terms are equal and the M(4,4) and M(5,5) terms are also equal. It is seen that the M(1,1) term is larger than the M(2,2) and M(3,3) terms which, in turn, are larger than the M(4,4) and M(5,5) terms. The M(1,1) term is positive and the other terms are negative. It is interesting to note that the apparent mass terms due to the corrected pressure distribution are always smaller than the apparent mass associated with the uncorrected pressure distributions. This can possibly be explained by the fact that with the corrected pressure distribution the lift tends towards the edge of the disc, while for the uncorrected pressure distribution it tends towards the hub.

To understand the difference between the complex L-matrix as calculated by S.P. and S.V. methods, it is better to compare the magnitude and phase angles of the complex elements for each method.

Figure 3 presents the magnitude of the (1,1) element of the complex L-matrix as calculated by each theory for a corrected thrust distribution. The S.V. magnitudes are calculated for discrete K values over the range of interest. The S.P. magnitudes are obtained form the square root of the sum of the squares of the real and imaginary terms. The real part, shown on figure 3 as a dot-dashed line, is the (1,1) term of the inverted steady L-matrix for $\alpha = 90^{\circ}$, table 1. The imaginary term for the S.P. method, shown as the large dashed line, is the apparent mass M(1,1), table 2, multiplied by the reduced frequency K. The combined magnitude of the real and imaginary parts are shown as the dotted line. When the lines of the real or imaginary component coalesce with the magnitude line, then the perspective component is predominantly larger than the other term. The maximum difference between the S.P. and S.V. theories is for the case of corrected thrust loading in the range of $1 \leq K \leq 10$. The maximum difference is close to 50%. Therefore, we conclude that either theory may deviate by $\pm$ 20% from the true value at K = 3. Although this is larger than originally hoped, especially since this is the range of most interest, we recall that the effect of dynamic inflow is itself a correction factor. Thus, error of 20% in a correction term may be acceptable. The agreement between the two methods improved for the uncorrected thrust loading which is not shown. Also not shown, but noted, was that the agreement for the first harmonic terms, columns 2 and 3, was better than that shown in figure 3. The best agreement was for the second harmonic terms, columns 4 and 5.

To fully understand the behavior of the inverted complex L-matrix, it is beneficial to look also at the phase angle variation of each element as a function of reduced frequency. The phase angle can be considered to be a time lag between the in-phase and out-of-phase induced velocities. The phase angle is the arc tangent of the ratio of the imaginary part to the real part. For the S.P. method, the real part is the inverted, steady L-matrix; and the imaginary term is the apparent mass multiplied by the reduced frequency. The phase angle for S.V. is defined as the arc tangent of the ratio of the imaginary part to the real part of the inverted complex L-matrix obtained by integration of the complex induced velocities of equation 15.

The phase angles for both the S.P. and S.V. solutions of the (1,1) element with a corrected thrust distribution are presented in figure 4. The S.V. method phase angle is larger than that of the S.P. method for $K < 5$ and greater than the S.P. phase angle for $K > 5$. The maximum deviation is $\pm 5^o$, which is quite acceptable; and the deviation is even less in the region of most interest $2 < K < 8$. It is interesting that the phase angles of the S.P. and S.V. converge more slowly (as $K \to 0$ and $K \to \infty$) than do the magnitudes. The phase-angle plots of the other element show similar trends, and are presented in greater detail in reference 19.

Up to this point, the unsteady results presented are for the axial-flow case, $\alpha = 90^o$. A major part of this research is to determine the comparison of the complex L-matrix obtained by S.P. and S.V. as the angle of attack varies from $\alpha = 90^o$ to $\alpha = 0^o$. The inverted complex L-matrix obtained by the S.P. method consists of the superposition of the inverted steady L-matrix and the apparent mass matrix. The apparent mass matrix, is a diagonal matrix that is independent of the rotor angle-of-attack and is the complex part of the inverted matrix. The real part is the inverted steady L-matrix, which varies with angle of attack and the imaginary part is only the diagonal terms which vary with K.

Each of the 13 non-zero elements of $[L(K)]^{-1}$ has real and imaginary parts (i.e. magnitude and phase) that vary with both angle-of-attack and reduced frequency. Therefore, it is beyond the scope of this paper to study every element in detail. Instead, we will discuss the diagonal elements only from a qualitative standpoint (no figures); and we will present data for only the most important off-diagonal terms, (3,1) and (1,3). Quantitative results for all elements can be found in reference 19. First of all, the diagonal elements of $[L]^{-1}$, as calculated by the S.V. and S.P. methods, show similar comparisons for $\alpha \neq 90^o$ as they do for $\alpha = 90^o$. Therefore, deviations of only $\pm$ 5% to $\pm$ 20% are found. The off-diagonal terms, however, are a different story.

We recall that, for $\alpha \neq 90^o$, the S.P. method gives real off-diagonal terms (due to the steady $[L]^{-1}$; but it gives absolutely no imaginary off-diagonal terms since the [M] matrix remains diagonal. The S.V. method, on the other hand, produces fully complex off-diagonals. Figures 5 and 6 show magnitude and phase for the S.V. method. Although the S.P. result is not explicitly shown, it is easily inferred. For magnitude, it is a horizontal line through the $K = 0$ values (independent of K); and, for phase, the S.P. result is identically zero. The magnitude plot shows that the S.P. and S.V. methods give close results for $0 < k < 10$ (except for the "dips" in the S.V. curves); however as K increases to 30, the magnitude shows a linear increase that is not predicted by the S.P. theory.

The S.V. phase shows in figure 6 a significant deviation from the S.P. method which predicts a phase angle of zero degrees. There appears to be an unexplainable shift in the sign of the phase angle for $K = 3$. For $K > 5$, the S.V. result is a 40^o phase shift (relatively independent of α) which cannot be accounted for by S.P.

Although the above results tend to place the S.P. and S.V. comparisons in a bad light, the discrepancies must be placed in perspective. In particular, how do the deviations in S.P. and S.V. in the off-diagonal terms compare with the overall magnitude of the dominant, diagonal elements. Figures 7 and 8 plot the ratios of (3,1) and (1,3) elements to the (3,3) element of $[L]^{-1}$ for a corrected first column and uncorrected second and third columns. Figure 7 shows the magnitude of this ratio. The S.P. method predicts equal magnitudes for the two ratios at $\alpha = 30^{\circ}$, and the S.V. method shows relatively equal values near the S.P. result. The maximum deviation appears in the (3,1) term near K = 4 (50% difference) but the other points are all within .15 of each other (15% off the (3,3) term). Figure 8 is phase angle relationship with both the $\alpha = 30^{\circ}$ case and the limit as $\alpha \rightarrow 90^{\circ}$ are given. At $\alpha = 90^{\circ}$, all phase angles are in agreement with the dominant portion coming from the (3,3) term in the denominator. When $\alpha = 30^{\circ}$, little or no change takes place in the S.P. results, since the off-diagonal remains purely real. For the S.V. method, however, the phase deviates significantly for K > 3. The only positive note is that the phase deviation becomes larger as the magnitude becomes smaller. For example, at K = 20 the phase deviation is 50° (quite large) but the magnitude is only 20% of the (3,3) term. Furthermore, the most important applications of dynamic inflow are in the range 0 < K < 5; and in this range, the phase agreement is much better. Finally, we note that pitch-thrust coupling is not as important to ground- and air-resonance as are the diagonal terms. Therefore, the variations shown in figures 7 and 8 might be acceptable, given the great simplicity of the S.P. method over the S.V. method. We conclude that the variations between the S.P. and S.V. method are not large enough to warrant abandonment of the simple S.P. model.

3.3 Prescribed Wake

The previous results provide a measure of the accuracy of the assumption of superposition of pressures. In this section, we assess the accuracy of the assumption of an actuator disc. This is accomplished for quasi-steady (k = 0) case by comparing actuator disc results to these from a discrete vortex analysis (lifting-line theory) for a rotor with a finite number of blades. For such an analysis of an actual rotor, the induced flow may not be small with respect to the free-stream, consequently, there may be wake contraction and wake skew. To account for this in the actuator-disc theory, we follow the suggestion of reference 18 and replace the parameters v and α with generalized counterparts. For very small lift (the actuator-disc case) we have a nondimensional free-stream velocity, v, with components μ and $\bar{\lambda}$ in and out of the rotor plane

$$\mu = v \cos\alpha \qquad \bar{\lambda} = v \sin\alpha \tag{24}$$

$$v = \sqrt{\mu^2 + \bar{\lambda}^2} \quad , \qquad \alpha = \tan^{-1} \bar{\lambda}/\mu \tag{25}$$

We extend this to the lifting case by introducing a third parameter, $\bar{\nu}$, the induced flow. The extended definitions of v and α (v^* and α^*) become

$$v^* = \frac{\mu^2 + (\bar{\lambda}+\bar{\nu})(\bar{\lambda}+2\bar{\nu})}{\sqrt{\mu^2 + (\bar{\lambda}+\bar{\nu})^2}} \qquad \alpha^* = \tan^{-1} \frac{\bar{\lambda}+\bar{\nu}}{\mu} \tag{26}$$

where equations 26 result from momentum considerations. Although α can be quite small for a rotor in forward flight, α^* is generally larger than 10°.

A comparison of the lifting-line and actuator-disc results are given in figures 9 through 11. Generally, results for disc angle of attack (α*) greater than 20^o are well-converged. Results for $\alpha^* < 20^o$, however, are very hard to obtain (due to the close proximity of the rotor disc and the shed vorticity). Because of this, results $\alpha^* < 20^o$ are suspect.

Figure 9 compares the first column of the actuator disc L-matrix to that determined by the prescribed wake method. The actuator-disc theory predicts the (1,1) term to be a constant 0.5, and the lifting-line results support the result. There is also good agreement between the corrected actuator-disc and the lifting-line results for $\alpha^* > 20^o$. For low α's however, the correlation is lost, with the lifting-line predicting less fore-to-aft gradient as $\alpha^* \rightarrow 0^o$. The (2,1) term is zero for all theories. Experimental data, however, has never shown a reduction in fore-to-aft gradient with edgewise flow. Therefore, we tend to discount the lifting-line results for $\alpha^* < 20^o$.

Figure 10 gives the (2,2) and (3,2) elements. The (2,2) element, one of the most important, seems well-modeled by the actuator-disc theory. Interestingly, the (2,3) term has fairly constant value (.2) from lifting line, although it is zero in actuator disc. This is clearly a wake rotation term.

Figure 11 presents the (1,3), (2,3), and (3,3) terms. The (1,3) term shows excellent agreement (except at 18^o) between actuator-disc and lifting-line results. The (3,3) term (one of the most important for ground resonance, shows excellent comparison). The (3,2) term is the counterpart to the (2,3) wake rotation. It is consistent with a typical wake rotation, but is probably not important for dynamic inflow. Thus, there is a very encouraging agreement between actuator-disc and lifting-line theories.

4. Summary and Conclusions

Four different inflow models are used to calculate dynamic inflow derivatives. The model are:

(1) Steady Actuator Disc-Corrected and Uncorrected radial load distribution.

(2) Unsteady Actuator Disc-Superposition of Pressure (S.P.) for both the corrected and uncorrected radial load distributions.

(3) Unsteady Actuator Disc-Superposition of Velocities (S.V.) for both the corrected and uncorrected radial load distributions.

(4) Prescribed-Wake Model

The induced-velocity distribution for each inflow model is numerically integrated over the rotor disc to obtain the L-matrix. Models 1-3 provide both a standard 3X3 nonuniform inflow L-matrix, and an extended 5X5 L-matrix that includes second-harmonic velocities and loadings. The fourth model includes wake contraction, wake rotation, and finite number of blades and serves as a measure of accuracy for the simpler, actuator-disc models.

From the steady actuator disc research we can conclude:

(1) In axial flow (e.g. hover), the gains (elements of the 3X3 L-matrix) are identical to those obtained from simple momentum theory, and are independent of the radial lift distribution. The magnitude of the elements increase with increasing harmonic loading, i.e., L_{55} & $L_{44} > L_{33}$ & $L_{22} > L_{11}$.

(2) For a thrust loading and edgewise flow, the cosine harmonics of induced velocity, L(3,1) and L(5,1), are large with respect to the average value L(1,1). For the other loading conditions, at $\alpha = 0^{\circ}$, all the higher-harmonic elements of the L-matrix are small save for L(5,5).

(3) Both the 5X5 and 3X3 steady L-matrices are well behaved and invertible as α varies from 90° to 0°.

In the unsteady, actuator-disc research, the inverted complex L-matrices of the S.P. and S.V. methods are compared. The following are the conclusions from this phase of the research:

(1) The apparent mass terms (the M-matrix) for the uncorrected pressure distributions are identical to the apparent mass terms of an impermeable disc, but vary significantly with lift distribution. The uncorrected terms are always larger than the corrected values.

(2) The apparent mass terms are more sensitive to the lift distribution than the corresponding terms in the L-matrix.

(3) The apparent mass magnitude (for either corrected or uncorrected distributions) decrease with increasing harmonics of induced velocity.

(4) The apparent mass terms of the S.V. method approach those of the S.P. method at high reduced frequencies (K). However, for small K, the S.V. and S.P. apparent mass terms are considerably different.

(5) For $\alpha \neq 90^{\circ}$ and $K > 0$, the S.V. method predicts imaginary terms for some of the off-diagonal elements while the S.P. method does not. However. these are small with respect to the diagonal terms.

The conclusions of the prescribed-wake program are:

(1) The prescribed-wake L-matrix agrees favorably with the L-matrix from the actuator-disc model, provided that the V and α^{*} parameters are considered.

(2) The prescribed-wake L-matrix has antisymmetric or cross coupling terms, L(3,2) and L(2,3), which are constant with α. These are not predicted by the Actuator-Disc Theory. These are due to the wake rotation associated with lifting rotor. For realistic values of rotor power, however, these are only 10 percent as large as the diagonal terms.

REFERENCES

1) K. B. Amer: Theory of Helicopter Damping in Pitch or Roll and Comparison with Flight Measurement.
NACA TN-2136, October 1948.

2) G. J. Sissingh: The Effect of Induced Velocity Variation on Helicopter Rotor Damping in Pitch or Roll.
Aeronautical Research Council (Great Britain), A.R.C. Technical Report C.P. No. 101 (14, 757), 1952.

3) P. J. Carpenter and B. Fridovitch: Effect of a Rapid Blade Pitch Increase on the Thrust and Induced Velocity Response of a Full Scale Helicopter Rotor.
NACA TN 3044, November 1953.

4) Jean Rebont, Jacques Valensi, and Jean Soulez-Lariviere: Response of a Helicopter Rotor to an Increase in Collective Pitch for the Case of Vertical Flight.
NASA TTF-55, 1961.

5) R. G. Loewy: A Two-Dimensional Approach to the Unsteady Aerodynamics of Rotary Wings.
Journal of Aerospace Science, Vol. 24, 1957, pp 82-98.

6) N. K. Shupe: A Study of the Dynamic Motions of Hingeless Rotored Helicopters.
Ph.D. Thesis, Princeton University, 1970.

7) R. A. Ormiston and D. A. Peters: Hingeless Helicopter Rotor Response with Nonuniform Inflow and Elastic Blade Bending.
Journal of Aircraft, Vol. 9, No. 10, October 1972.

8) S. T. Crews, K. H. Hohenemser, and R. A. Ormiston: An Unsteady Wake Model for a Hingeless Rotor.
Journal of Aircraft, Vol. 10, No. 12, December 1973.

9) D. A. Peters: Hingeless Rotor Frequency Response with Unsteady, Inflow.
Presented at the AHS/NASA - Ames Specialists' Meeting on "Rotorcraft Dynamics", NASA SP-362, February 1974.

10) D. Banerjee, S. T. Crews, and K. H. Hohenemser: Parameter Identification Applied to Analytic Hingeless Rotor Modeling.
JAHS, Vol. 24, No. 1, January 1979, pp 26-32.

11) R. A. Ormiston: Application of Simplified Inflow Models to Rotorcraft Dynamic Analysis.
JAHS, Vol. 21, No. 3, July 1976.

12) D. A. Peters and G. H. Gaonkar: Theoretical Flap-Lag Damping with Various Dynamic Inflow Model.
JAHS, Vol. 25, No. 3, July 1980.

13) G. H. Gaonkar, et al: Sensitivity of Helicopter Aeromechanical Stability to Dynamic Inflow.
Vertica, Vol. 6, No. 1, 1982.

14) Wayne Johnson: The Influence of Variable Inflow on Hingeless Rotor Ground Resonance.
NASA TM-81302, July 1981.

15) M. Joglekar and R. Loewy: An Actuator-Disc Analysis of Helicopter Wake Geometry and the Corresponding Blade Response.
USAAVLABS Technical Report 69-66, 1970.

16) A. J. Landgrebe and T. A. Egolf: Rotorcraft Wake Analysis for the Prediction of Induced Velocities.
USAAMRDL Technical Report 75-45, U.S. Army Mobility Research and Development Laboratory, Fort Eustis, Virginia, January 1976.

17) R. A. Ormiston: An Actuator-Disc Theory for Rotor Wake Induced Velocities.
Presented at the AGARD Specialists' Meeting on the "Aerodynamics of Rotary Wings", Marseilles, France, September 13-15, 1972.

18) D. M. Pitt and D. A. Peters: Theoretical Prediction of Dynamic-Inflow Derivatives.
Presented at the Sixth European Rotorcraft and Powered Lift Aircraft Forum, Bristol, England, September 1980. Also published in Vertica.

19) D. M. Pitt: Rotor Dynamic Inflow Derivative and Time Constants from Various Inflow Models.
Doctor of Science Thesis, Washington University, St. Louis, Missouri, December 1980. Also published as USATSARCOM Technical Report TR81-2.

20) G. H. Gaonkar, V. V. S. S. Sastry, T. S. R. Reddy, J. Nagabhushanam, and D. A. Peters: The Use of Actuator-Disc Dynamic Inflow for Helicopter Flap-Lag Stability.
JAHS, Vol. 28. No. 3, July 1983.

L-MATRIX ELEMENTS

ELEMENT	UNCORRECTED	CORRECTED	MOMENTUM
L_{11}	1/2	1/2	.5
L_{22}	$\frac{-4}{(1+\sin\alpha)}$	$\frac{-4}{(1+\sin\alpha)}$	-2
L_{33}	$\frac{-4\sin\alpha}{(1+\sin\alpha)}$	$\frac{-4\sin\alpha}{(1+\sin\alpha)}$	-2
L_{44}	$\frac{-\sin\alpha(11-5\sin\alpha)}{(1+\sin\alpha)}$	$\frac{-\sin\alpha(11-5\sin\alpha)}{(1+\sin\alpha)}$	0
L_{55}	$\frac{-6(1+\sin^2\alpha)}{(1+\sin\alpha)^2}$	$\frac{-6(1+\sin^2\alpha)}{(1+\sin\alpha)^2}$	0
L_{31}	$\frac{3\pi}{8}\ \frac{(1-\sin\alpha)}{(1+\sin\alpha)}$	$\frac{15\pi}{64}\ \frac{(1-\sin\alpha)}{(1+\sin\alpha)}$	0
L_{13}	$\frac{15\pi}{64}\ \frac{(1-\sin\alpha)}{(1+\sin\alpha)}$	$\frac{525\pi}{2048}\ \frac{(1-\sin\alpha)}{(1+\sin\alpha)}$	0
L_{51}	$\frac{3}{5}\ \frac{(1-\sin\alpha)}{(1+\sin\alpha)}$	$-\frac{3}{7}\ \frac{(1-\sin\alpha)}{(1+\sin\alpha)}$	0
L_{42}	$-\frac{45\pi}{32}\ \frac{(1-\sin\alpha)}{(1+\sin\alpha)}$	$-\frac{2205\pi}{2048}\ \frac{(1-\sin\alpha)}{(1+\sin\alpha)}$	0
L_{24}	$\frac{105\pi}{128}\ \frac{(1-\sin\alpha)}{(1+\sin\alpha)}$	$\frac{105\pi}{128}\ \frac{(1-\sin\alpha)}{(1+\sin\alpha)}$	0
L_{53}	$-\pi\sin\alpha(1-\sin\alpha)$	$-\frac{3\pi}{4}\sin\alpha(1-\sin\alpha)$	0
L_{35}	$2\sin\alpha(1-\sin\alpha)$	$2\sin\alpha(1-\sin\alpha)$	0

Multiply all elements by 1/v
All other elements not shown are zero

TABLE 1

Elements of M-Matrix

Element	Uncorrected	Corrected
M_{11}	$\frac{8}{3\pi} = .8488$	$\frac{128}{75\pi} = .5432$
$M_{22} = M_{33}$	$-\frac{16}{45\pi} = -.1132$	$-\frac{256}{945\pi} = -.0862$
$M_{44} = M_{55}$	$-\frac{256}{1575\pi} = -.0517$	-
M_{ij}, $i \neq j$	0	0

TABLE 2

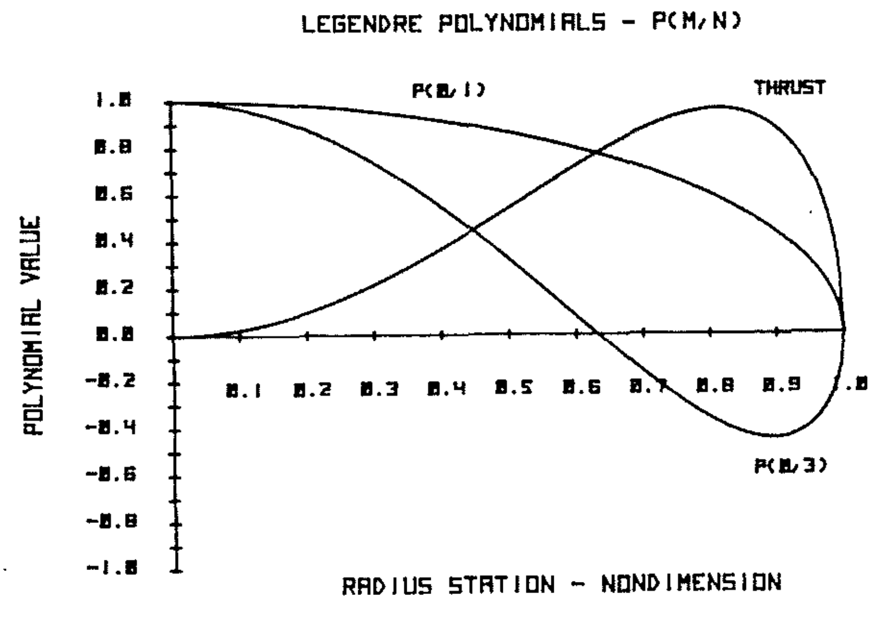

'igure 1. Corrected (Thrust) and Uncorrected (P_1^0) Lift Distribution for C_T.

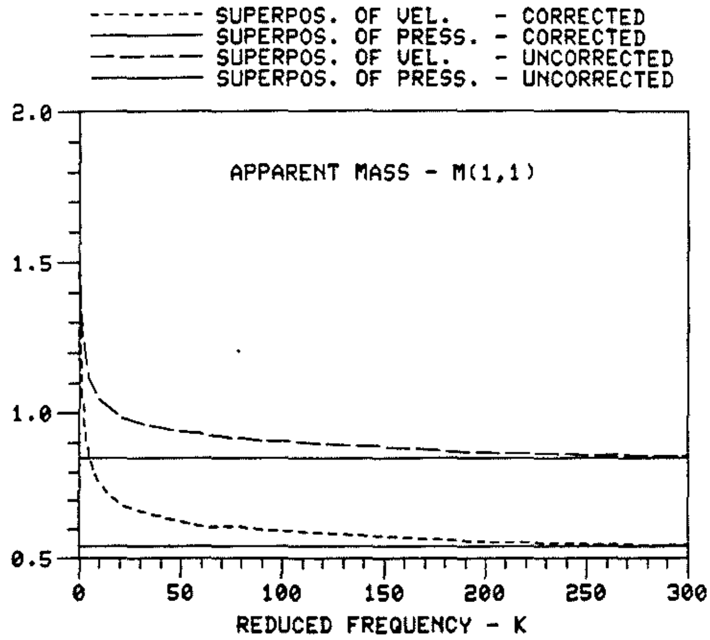

Figure 2. Apparent Mass Element M(1,1) for $\alpha = 90^{o}$

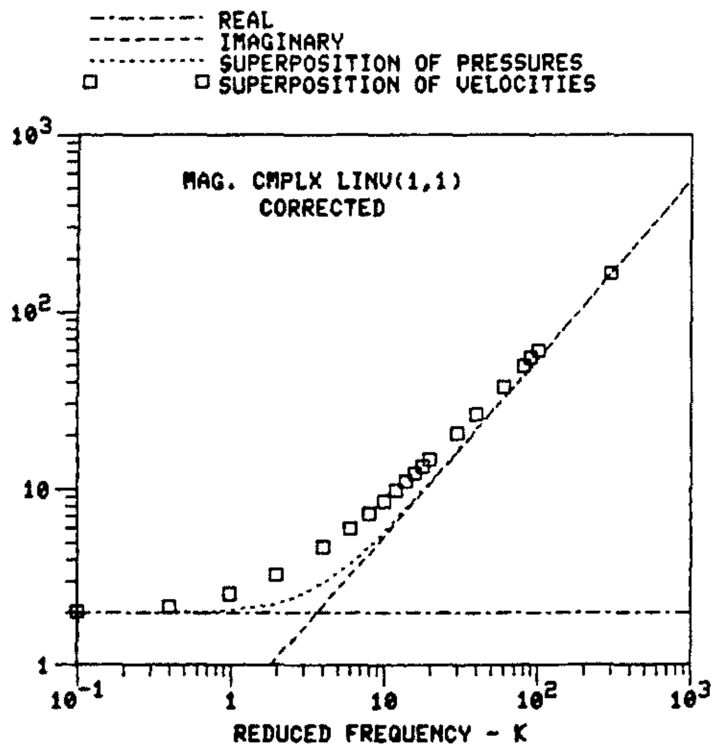

Figure 3. Magnitude of the (1,1) Element of Inverted Complex L(K) Matrix at $\alpha = 90^{o}$ with Corrected Pressure

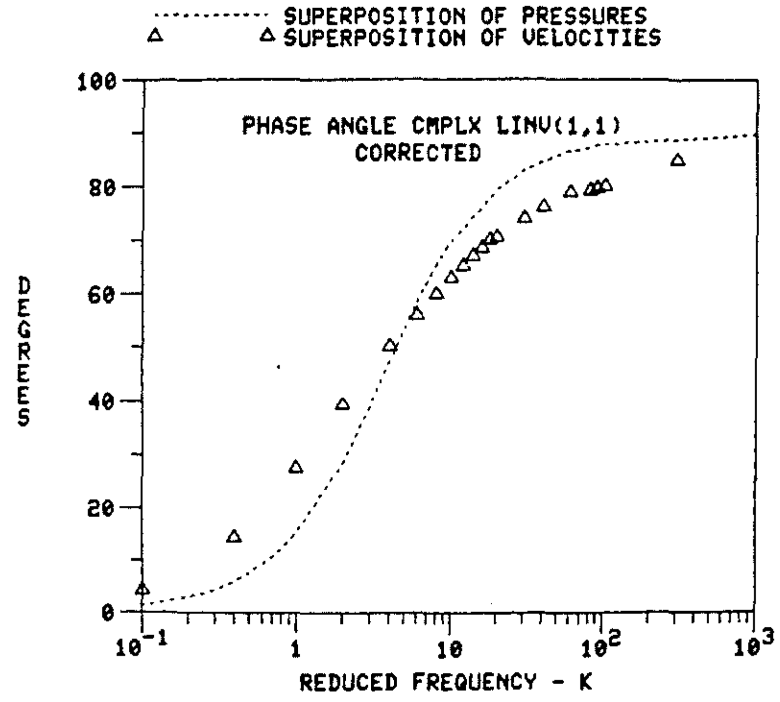

Figure 4. Phase Angle of the (1,1) Element of Inverted Complex L(K) Matrix at $\alpha = 90^o$ with Corrected Pressure Distribution

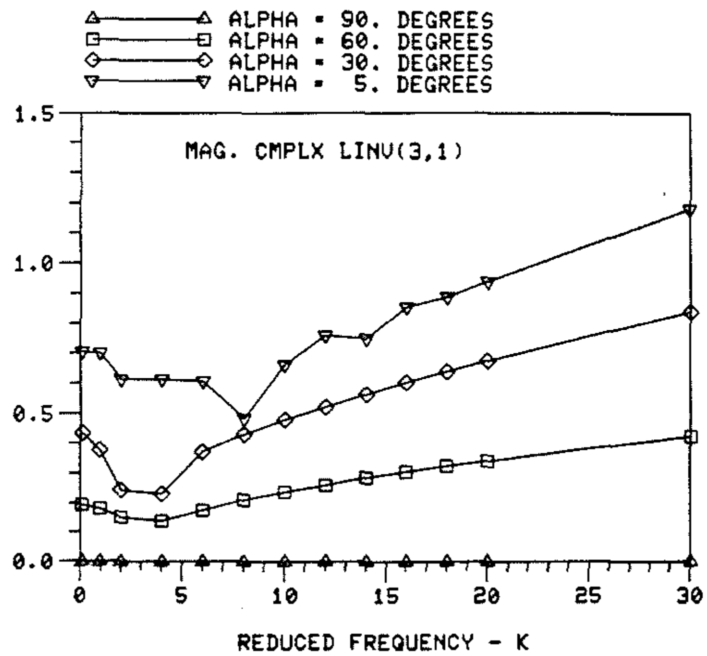

Figure 5. Magnitude of the (3,1) Element of Inverted Complex L(K) Matrix for α Sweep (Corrected Pressure)

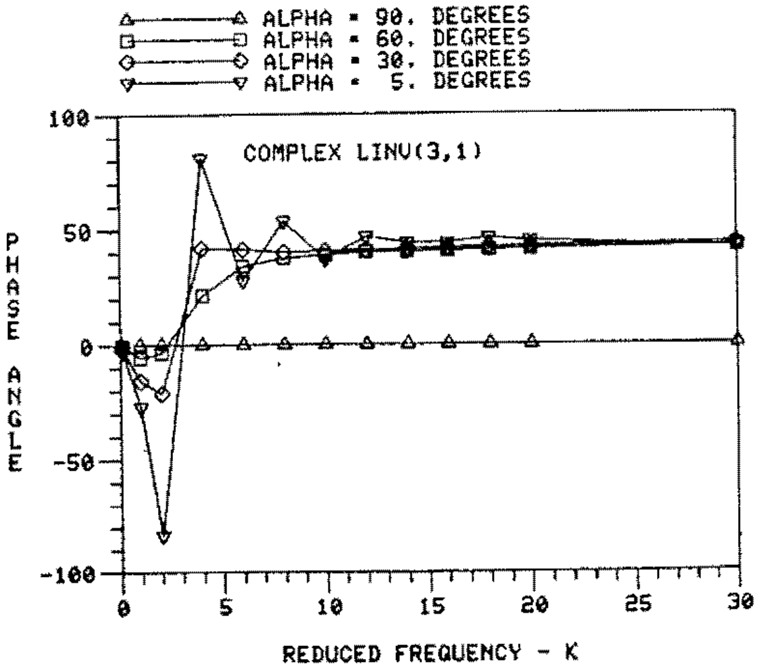

Figure 6. Phase Angle of the (3,1) Element of Inverted Complex L(K) Matrix for α Sweep (Corrected Pressure)

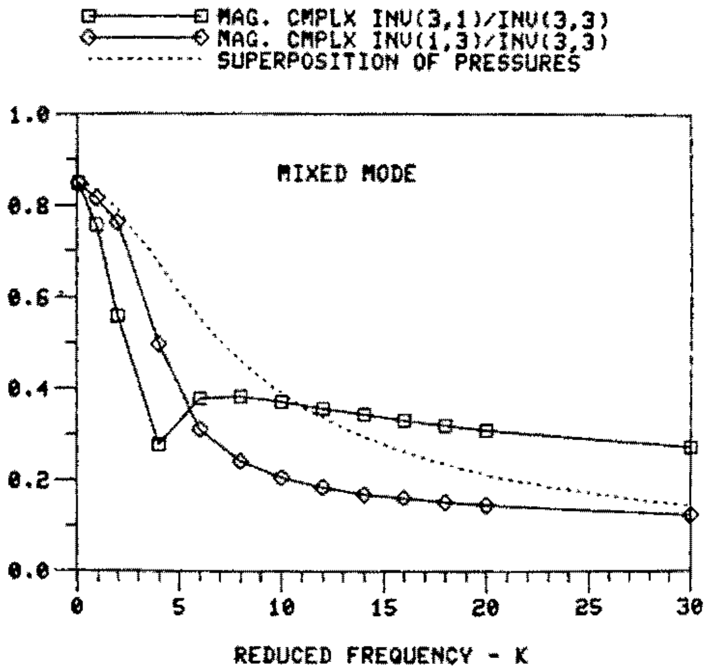

Figure 7. Relative Magnitude of the Off-Diagonal Terms of the 3X3 Inverted Complex L(K) Matrix at $\alpha = 30^{\circ}$

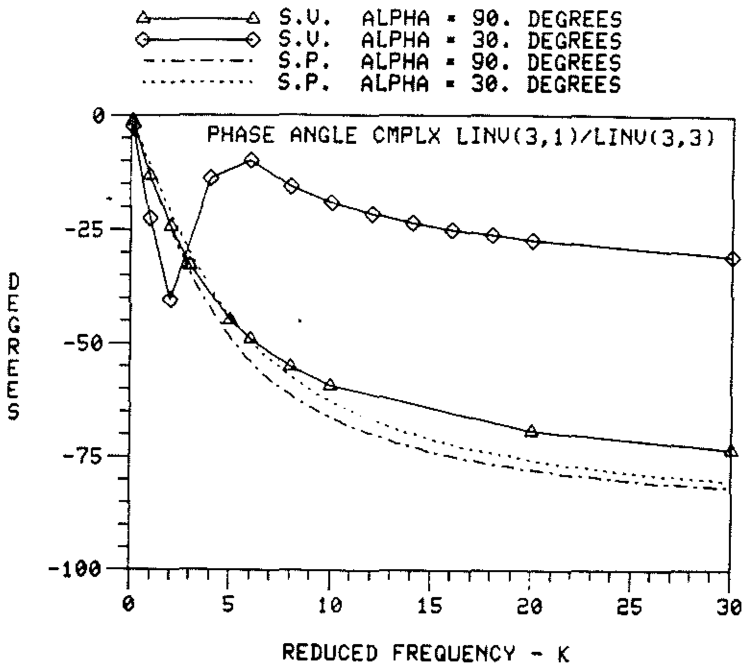

Figure 8. Phase Angle of Complex (3,1)/(3,3) for Analytical L and M Matrices

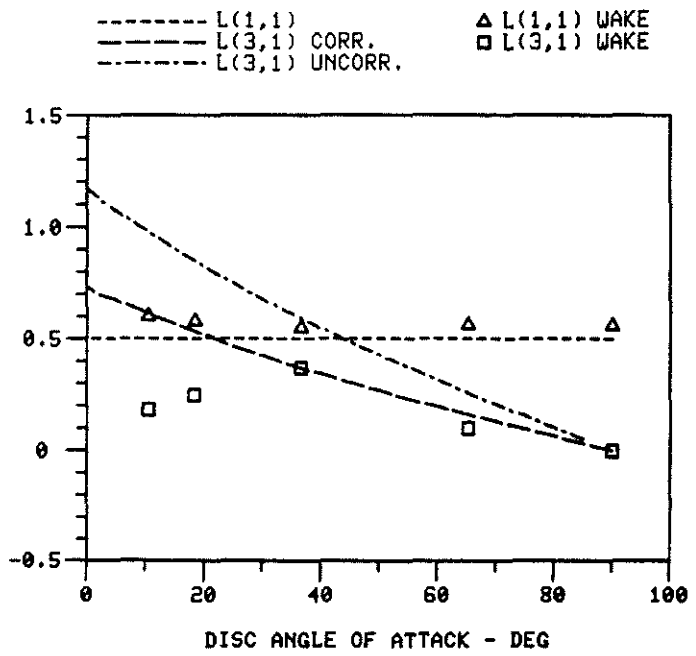

Figure 9. First Column of the Prescribed-Wake L-Matrix

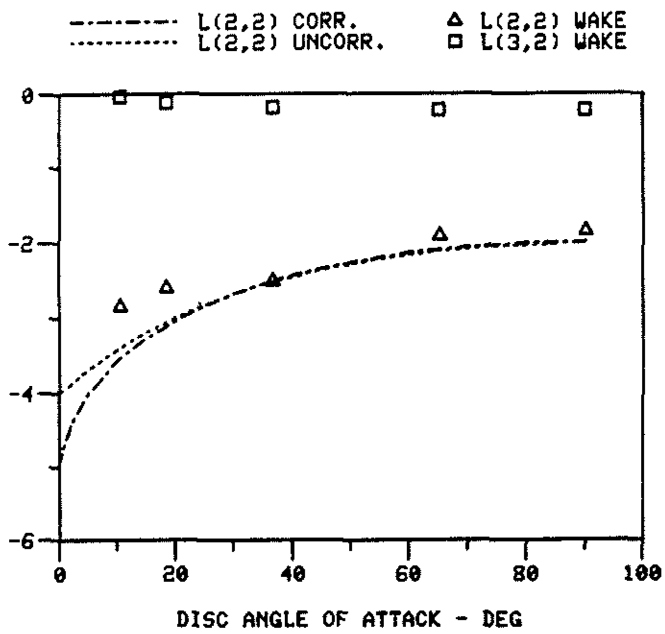

Figure 10. Second Column of the Prescribed-Wake L-Matrix

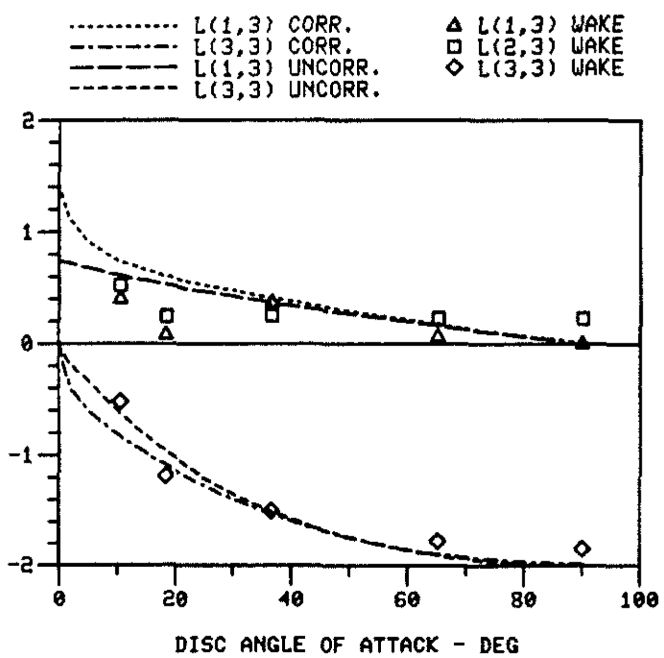

Figure 11. Third Column of the Prescribed-Wake L-Matrix